Optical conductivity and x-ray absorption spectra of the Mott-Hubbard compounds RVO_3 (R=Sr, Ca, La, and Y)

R. J. O. Mossanek,[1] M. Abbate,[1] P. T. Fonseca,[2] A. Fujimori,[3] H. Eisaki,[4] S. Uchida,[5] and Y. Tokura[6]
[1]*Departamento de Física, Universidade Federal do Paraná, Caixa Postal 19081, 81531-990 Curitiba, Paraná, Brazil*
[2]*Laboratório Nacional de Luz Síncrotron, Caixa Postal 6192, 13083-970 Campinas, São Paulo, Brazil*
[3]*Department of Complexity Science and Engineering, University of Tokyo, Kashiwa, Chiba 277-856, Japan*
[4]*Nanoelectronics Research Institute, AIST, 1-1-1 Central 2, Umezono, Tsukuba, Ibaraki 305-8568, Japan*
[5]*Department of Physics, University of Tokyo, Tokyo 113-0033, Japan*
[6]*Department of Applied Physics, University of Tokyo, Tokyo 113-8656, Japan*
(Received 12 August 2009; published 6 November 2009)

Core-level and valence-band optical spectra provide important information on highly correlated systems. The former corresponds to transitions from the core level to the conduction band, and it is usually related to the unoccupied electronic structure. The later corresponds to transitions from the valence band to the conduction band, and it is sometimes described in terms of the joint density of states. These spectra are usually treated separately due to the differences in the experimental and theoretical methods. We present here a combined description of the core-level and valence-level optical spectra of Mott-Hubbard compounds. In particular, we studied the O 1*s* x-ray absorption and the optical-conductivity spectra of $SrVO_3$-$CaVO_3$-$LaVO_3$-YVO_3. The experimental data were analyzed using an extended *p-d* cluster model solved by an exact diagonalization method. The results show that correlation effects alone cannot account for the experimental structures, and that crystal-field effects and exchange interactions are necessary to explain the spectra. We also show that there is a correspondence between the features in the charge-transfer region of both spectra.

DOI: 10.1103/PhysRevB.80.195107 PACS number(s): 78.70.Dm, 71.30.+h, 78.20.Bh

I. INTRODUCTION

Understanding highly correlated systems is one of the main challenges in condensed-matter physics. For instance, great efforts were devoted to elucidate the electronic structure of transition-metal oxides. The motivation was to understand the microscopic origin of their fascinating physical properties. Core-level and valence-band optical spectra provided important information on high-T_C superconductors,[1] colossal magnetoresistance materials,[2] and Mott-Hubbard systems.[3]

The core-level optical spectra correspond to transitions from a core level to the conduction band. In a first approximation, these spectra are usually explained in terms of the unoccupied electronic structure. The O 1*s* x-ray absorption spectra (XAS) revealed the nature of the doped states in high-T_C superconductors,[4] the oxidation state in colossal magnetoresistance materials,[5] and the unoccupied 3*d* bands in Mott-Hubbard systems.[6–8]

The valence-band spectra correspond to transitions from the valence band to the conduction band. The spectra are usually described in terms of joint density of states or current-current correlation functions. The optical-conductivity spectra revealed an anomalous behavior in high-T_C superconductors,[9] the exchange splitting in colossal magnetoresistance oxides,[10] and correlation effects in Mott-Hubbard systems.[11–13]

The core-level and valence-band optical spectra are seldom discussed in the same work,[14] mostly because of the differences in both the experimental and theoretical methods. We present here the O 1*s* x-ray absorption and optical-conductivity spectra of the $SrVO_3$-$CaVO_3$-$LaVO_3$-YVO_3 series. The results show that the distribution of spectral weight is sensitive to crystal field and exchange interactions. Further, there is a correspondence of the spectral weight in the charge-transfer region of these spectra.

The electronic structure of these compounds was studied using a wide variety of theoretical methods. The band structure of $LaVO_3$ and YVO_3 was studied using the generalized gradient approximation and LDA+U approaches (LDA: local-density approximation).[15,16] The electronic structure of metallic $SrVO_3$ and $CaVO_3$ was investigated with the LDA +DMFT method.[17] The same method was used to study the electronic structure of insulating $LaVO_3$ and YVO_3.[18] The spectral weight of these materials was also studied using an extended cluster model.[8,19]

The $SrVO_3$ and $CaVO_3$ compounds are paramagnetic metals with a nominal occupation of $3d^1$ (V^{4+}). The V-O-V angle decreases from 180° in $SrVO_3$ to 160° in $CaVO_3$ reducing the effective V 3*d* bandwidth. The $LaVO_3$ and YVO_3 materials are antiferromagnetic insulators with a nominal valence of $3d^2$ (V^{3+}). The larger band filling inhibits the metallic charge fluctuations producing a metal-insulator transition. The V-O-V angle decreases from 158° in $LaVO_3$ to 144° in YVO_3, reducing the one-electron bandwidth.

II. CALCULATION DETAILS

A periodic lattice model can be mapped into a correlated impurity site embedded in an effective medium. In the dynamical mean-field theory (DMFT), the self-energy $\Sigma(\omega)$ of the impurity site and the effective medium is obtained self-consistently.[20,21] Alternatively, the effective medium can be described by adjustable parameters as in the extended cluster model.[22–24] This model was already applied to

high-T_C superconductors,[22] colossal magnetoresistance materials,[23] and Mott-Hubbard systems.[24]

The model Hamiltonian can be separated into the intracluster and intercluster components: $H=H_{\text{intra}}+H_{\text{inter}}$. The intracluster part describes the p-d charge fluctuations within a single regular VO_6 octahedron,

$$H_{\text{intra}} = \sum_{m,\sigma} \varepsilon^{d}_{m,\sigma} d^{+}_{m,\sigma} d_{m,\sigma} + \sum_{m,\sigma} \varepsilon^{p}_{m,\sigma} p^{+}_{m,\sigma} p_{m,\sigma} + \sum_{m,\sigma,m',\sigma'} (U - J\delta_{\sigma,\sigma'}) d^{+}_{m,\sigma} d_{m,\sigma} d^{+}_{m',\sigma'} d_{m',\sigma'} + \sum_{m,\sigma} T_m (d^{+}_{m,\sigma} p_{m,\sigma} + \text{H.c.}), \quad (1)$$

where $d^{+}_{m\sigma}$ ($p_{m\sigma}$) creates (annihilates) a V $3d$ (O $2p$) electron with energy $\varepsilon^{d}_{m\sigma}$ ($\varepsilon^{p}_{m\sigma}$). The index m refers to the orbital symmetry and the index σ denotes the different spins.

The intercluster contribution in the $SrVO_3$ and $CaVO_3$ materials corresponds to charge fluctuation from a coherent state. The metallic intercluster Hamiltonian is given by

$$H^{met}_{\text{inter}} = \sum_{m,\sigma} \varepsilon^{C}_{m,\sigma} C^{+}_{m,\sigma} C_{m,\sigma} + \sum_{m,\sigma} T^{*}_{m} (d^{+}_{m,\sigma} C_{m,\sigma} + \text{H.c.}), \quad (2)$$

where $C^{+}_{m\sigma}$ creates a coherent electron with energy $\varepsilon^{C}_{m\sigma}$.

On the other hand, the intercluster contribution in the insulating $LaVO_3$ and YVO_3 compounds corresponds to Mott-Hubbard charge fluctuations. The insulating intercluster Hamiltonian is given by

$$H^{ins}_{\text{inter}} = \sum_{m,\sigma} \varepsilon^{D}_{m,\sigma} D^{+}_{m,\sigma} D_{m,\sigma} + \sum_{m,\sigma} T'_{m} (d^{+}_{m,\sigma} D_{m,\sigma} + \text{H.c.}), \quad (3)$$

where $D^{+}_{m\sigma}$ creates an electron in the nearest-neighbor V $3d$ state with energy ($\varepsilon^{D}_{m,\sigma}$).

The main parameters of the intracluster contribution are: the p-d charge-transfer energy $\Delta=\varepsilon^{d}-\varepsilon^{p}+U$, the d-d Mott-Hubbard energy U, and the symmetry-dependent p-d hybridization T_m.[25] The multiplet splitting is caused by crystal-field effects (10Dq), intra-atomic exchange (J), and the p-p transfer integral ($pp\pi-pp\sigma$).[26]

The metallic intercluster parameters are the coherent charge-transfer energy $\Delta^{*}=\varepsilon^{d}-\varepsilon^{C}+U$, and the effective hybridization with the coherent states T^{*}.[22–24] On the other hand, the insulating intercluster parameters are the Mott-Hubbard charge-transfer $\Delta'=\varepsilon^{d}-\varepsilon^{D}+U$, and the hybridization with the nearest-neighbor V $3d$ state T'.[26] The values of the parameters listed in Table I are the same used to explain the photoemission spectra of these compounds.[26]

Figure 1 depicts the different charge fluctuations in the metallic and insulating phase. The intracluster transitions from the O $2p$ states (Δ,T) are present in both phases. The metallic intercluster fluctuations, top panel, correspond to transitions from coherent states (Δ^{*},T^{*}). These coherent fluctuations are related to the low-energy excitations in the metallic phase. Finally, the insulating intercluster part, bottom panel, represents transitions from a nearest-neighbor V $3d$ state (Δ',T').

TABLE I. Parameters used in the extended cluster model calculations (all values in eV).

	$SrVO_3$	$CaVO_3$	$LaVO_3$	YVO_3
Δ	2.0	2.0	3.8	3.8
U	5.0	5.0	4.2	4.2
$pd\sigma$	1.9	1.6	1.8	1.5
10Dq	1.8	1.5	1.8	1.5
J	0.40	0.40	0.50	0.60
$pp\pi-pp\sigma$	0.80	0.80	0.80	0.80
Δ^{*}	0.75	0.55		
T^{*}	0.27	0.22		
Δ'			4.2	4.2
T'			0.42	0.36

The Hamiltonian is solved by exact diagonalization within the configuration-interaction method. The different removal (addition) states are obtained by removing (adding) an electron from (to) the ground state. Finally, the removal $A^{N-1}(\omega)$ and addition $A^{N+1}(\omega)$ spectra are obtained using

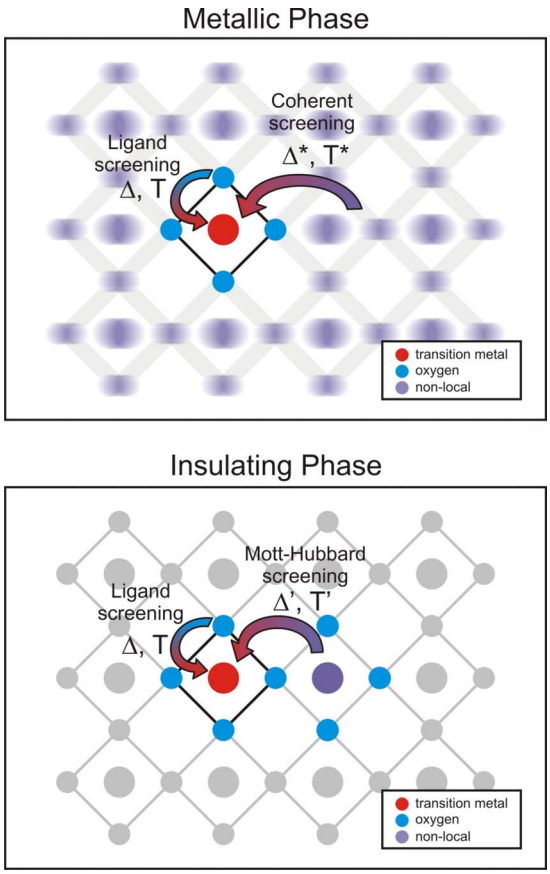

FIG. 1. (Color online) Schematic representation of the extended cluster model. In the metallic phase (top panel) the charge fluctuations considered are the intracluster ligand screening and the intercluster coherent screening. In the insulating phase (bottom panel) the charge fluctuations considered are the intracluster ligand screening and the intercluster Mott-Hubbard screening.

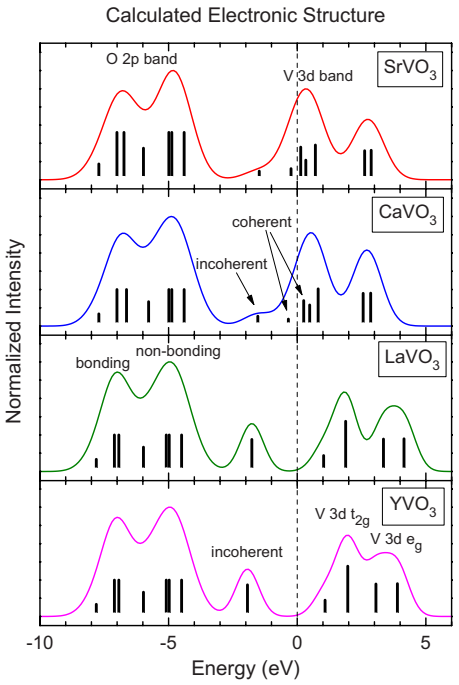

FIG. 2. (Color online) Calculated electronic structure of $SrVO_3$-$CaVO_3$-$LaVO_3$-YVO_3. The calculation is composed by the removal and addition spectra. The O $2p$ band is formed by the O $2p$-V $3d$ bonding and O $2p$ nonbonding parts. The V $3d$ band contains the coherent and incoherent structures in the metallic phase, and only the incoherent feature in the insulating phase. The unoccupied V $3d$ band is mostly split by crystal-field effects into the V t_{2g} and V e_g subbands.

the sudden approximation.[26] The discrete transitions were further convoluted with a Gaussian to include the band dispersion.

III. EXPERIMENTAL DETAILS

The $SrVO_3$, $CaVO_3$, $LaVO_3$, and YVO_3 samples were single crystals grown by the floating-zone method. The samples presented a single phase structure as established by powder x-ray diffraction. The chemical composition was confirmed using x-ray photoelectron spectroscopy (XPS).[26] The O $1s$ XAS were measured at the SGM beam line in the LNLS, Brazil. The spectra were taken in the total-electron yield method by measuring the drift current. The base pressure was around 5×10^{-9} mbar and the samples were kept at room temperature. The energy resolution was set to around 0.5 eV and the energy scale was calibrated with reference samples. The samples were repeatedly scrapped with a diamond file to remove any surface contamination, as confirmed by analyzing the O $1s$ XPS spectra.[26] The spectra were normalized to the maximum after the subtraction of the background.

IV. RESULTS AND DISCUSSION

A. Spectral-weight distribution

Figure 2 shows the calculated electronic structure of the $SrVO_3$-$CaVO_3$-$LaVO_3$-YVO_3 compounds. The total spectral weight is the combination of the removal (valence-band) and addition (conduction-band) states.

The removal spectra present the O $2p$ bands, from −8 to −3 eV, and the V $3d$ bands, from −3 to 0 eV. The O $2p$ bands do not change much across the series and are formed by an O $2p$-V $3d$ bonding region, around −7 eV, and an O $2p$ nonbonding part, about −5 eV. Contrarily, the V $3d$ bands change drastically from the metallic $SrVO_3$-$CaVO_3$ to the insulating $LaVO_3$-YVO_3 compounds. The V $3d$ bands in the metallic systems present an incoherent peak, around −1.6 eV, and a coherent peak, about −0.2 eV. On the other hand, the coherent peak disappears in the insulating compounds, and the incoherent peak shifts to lower energies, around 1.9 eV.[26] The spectral weight in the V $3d$ band region follows the same trend observed in LDA+DMFT.[17,18]

The addition spectra present the V $3d$ bands, from 0 to 5 eV, which are split by crystal field and exchange interactions. In the metallic compounds, the V $3d$ bands are split into the t_{2g}, around 0.5 eV and e_g, about 3 eV, subbands. Further, the coherent contribution to the addition spectra appears just above the Fermi level, within the t_{2g} region. The coherent component vanishes in the insulating compounds and the t_{2g} and e_g subbands are shifted to higher energies, around 2 and 4 eV. The disappearance of the coherent contribution in both the removal and addition spectra opens the band gap in $LaVO_3$-YVO_3.[26]

B. O 1*s* x-ray absorption spectra

Figure 3 shows the experimental and calculated O $1s$ x-ray absorption spectra of $SrVO_3$-$CaVO_3$-$LaVO_3$-YVO_3. These spectra correspond to transitions from the O $1s$ core level to unoccupied O $2p$ character in the conduction band. The calculated spectra were shifted 528.5 eV to take into account the binding energy of the O $1s$ core level. The intensity observed below 528 eV corresponds to the tail of the V $2p_{1/2}$ x-ray absorption peak.

The spectra of metallic $SrVO_3$ and $CaVO_3$ reflect the V t_{2g}, around 529 eV, and the V e_g subbands, about 531 eV. The crystal-field splitting determines the energy separation between the V t_{2g} and V e_g structures, around 2.1 eV. Each of these structures is further split by exchange interaction, about 0.4 eV, into the different spin states. The increasing intensities above 535 eV correspond to O $2p$ character mixed in the Sr $4d$ and Ca $3d$ bands. We note that the coherent contribution is strongly suppressed because the spectra reflect the unoccupied O $2p$ character.

The V t_{2g} and V e_g structures in insulating $LaVO_3$ and YVO_3 are shifted to higher energies, around 530 and 532 eV, respectively. In this case, the crystal-field splitting is around 2.3 eV and the exchange splitting increases to about 0.9 eV. Finally, the structures around 534 eV correspond to O $2p$ character mixed in the La $5d$ and Y $4d$ bands.

The calculated spectra reproduce the energy position and relative intensity of the experimental features. These results show that the O $1s$ XAS spectra are dominated by crystal field and exchange interactions. Thus, correlation effects alone are not able to reproduce the experimental features in the spectra.

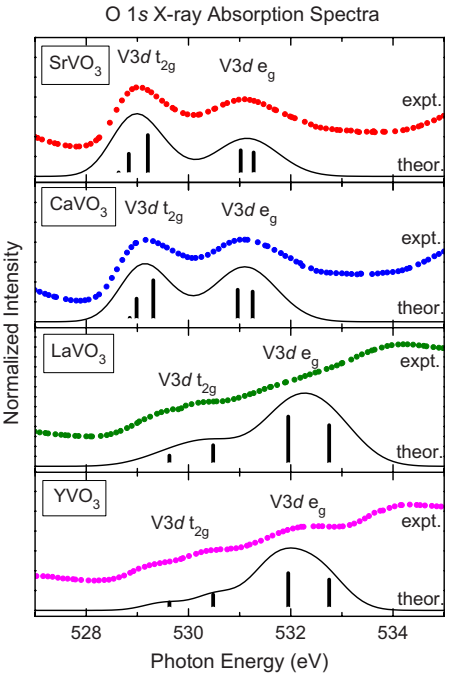

FIG. 3. (Color online) O 1*s* x-ray absorption spectra of $SrVO_3$-$CaVO_3$-$LaVO_3$-YVO_3. The spectra correspond to transitions from the O 1*s* core level to unoccupied O 2*p* states. The spectra reflect, via the O 2*p*-V 3*d* hybridization, the unoccupied V 3*d* bands, which are split into the V t_{2g} and V e_g subbands by crystal-field effects. Each of these subbands is further split by exchange interactions into the different spin states.

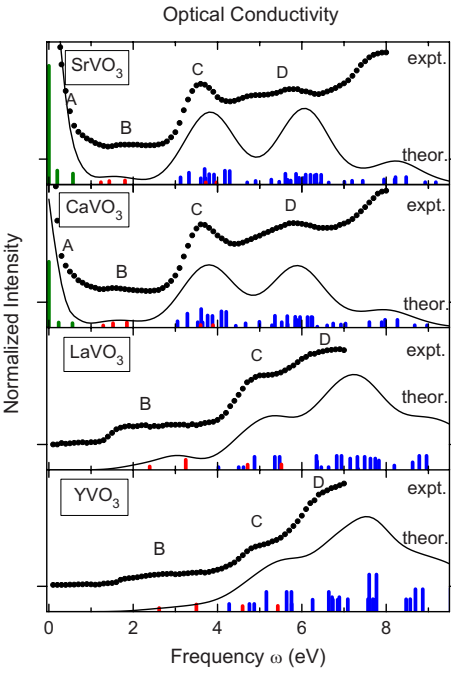

FIG. 4. (Color online) Optical-conductivity spectra of $SrVO_3$-$CaVO_3$-$LaVO_3$-YVO_3. The experimental spectra were taken from Refs. 12, 13, and 22. The metallic spectra present the Drude tail (A), a weak contribution (B), and the stronger charge-transfer transitions (C and D). The Drude contribution disappears in the insulating spectra giving a band gap of about 1.7 eV.

C. Optical conductivity

Figure 4 shows the experimental, taken from Refs. 12, 13, and 27, and calculated optical-conductivity spectra of $SrVO_3$-$CaVO_3$-$LaVO_3$-YVO_3. These spectra correspond to transitions from the valence band to unoccupied states in the conduction band.

The optical conductivity of the metallic $SrVO_3$ and $CaVO_3$ compounds present the Drude tail (A) below 1.0 eV. As expected, the overall intensity and width of the Drude contribution for $SrVO_3$ is larger than for $CaVO_3$. This was attributed to a larger correlation contribution to the effective mass for $CaVO_3$ than for $SrVO_3$.[12] The spectra present a relatively weak structure (B) around 1.7 eV and the much stronger charge-transfer transitions (C and D) about 3.5 and 5.5 eV.

On the other hand, the Drude tail disappears in the optical conductivity of the insulating $LaVO_3$ and YVO_3 compounds. The weak structure (B) starts around 1.7 eV, which defines the value of the optical gap, and its intensity is slightly larger than in the metallic $SrVO_3$ and $CaVO_3$ compounds. Finally, the much stronger charge-transfer features (C and D) are shifted to around 5.0 and 6.5 eV, respectively.

In lattice models, the optical conductivity is related to the Fourier transform of the current-current correlation function.[1] However, in local models, it is given by the correlation function between the removal $A^{N-1}(\omega)$ and addition $A^{N+1}(\omega)$ spectrum,[11]

$$\sigma(\omega) \propto \frac{1}{\omega}\int_{-\infty}^{\infty} A^{N-1}(\omega')A^{N+1}(\omega+\omega')d\omega'. \qquad (4)$$

The Drude contribution (A) is due to intraband transitions from the occupied to the unoccupied coherent states. The larger intensity of the Drude peak in the $SrVO_3$ material is due to the larger contribution from the coherent states. On the other hand, the regular contribution to the optical conductivity is mostly given by interatomic *p*-*d* transitions. The weak structure (B) is attributed to transitions from the incoherent peak to unoccupied V t_{2g} states whereas the corresponding transitions to unoccupied V e_g states are hidden beneath the much stronger feature (C). The charge-transfer transitions (C and D) come mostly from the nonbonding O 2*p* band to V t_{2g} and V e_g states, respectively. However, transitions from the bonding O 2*p*-V 3*d* band to unoccupied V t_{2g} states also contribute to feature (D). The energy separation between the V t_{2g} and V e_g charge-transfer structures are thus related to the crystal-field splitting.

We note that the onset of the charge-transfer features in the optical-conductivity scales with the charge-transfer energy Δ. The value of this parameter is around 2 eV for metallic $SrVO_3$-$CaVO_3$ and about 4 eV for insulating $LaVO_3$-YVO_3. Thus, the increase in Δ helps to explain the shift of the charge-transfer transitions in the insulating compounds. We also note that the experimental structures are at slightly lower energies than in the calculated spectra. This energy discrepancy is attributed to excitonic effects, which are not included in the present calculation.

D. Charge-transfer transitions

Figure 5 compares the optical conductivity, taken from Refs. 12, 13, and 27, and the O 1*s* x-ray absorption spectra

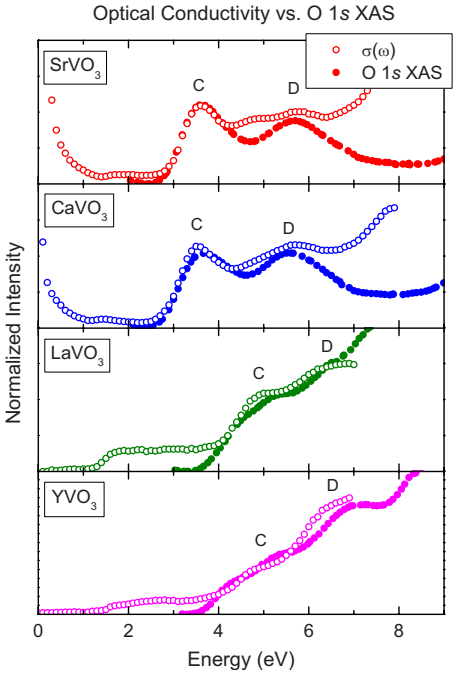

FIG. 5. (Color online) Comparison of the O 1*s* x-ray absorption and optical-conductivity spectra of $SrVO_3$-$CaVO_3$-$LaVO_3$-YVO_3, taken form Refs. 12, 13, and 27. There is a correspondence in the charge-transfer region of the spectra, mostly because both the spectra correspond to transitions to unoccupied V t_{2g} and V e_g states.

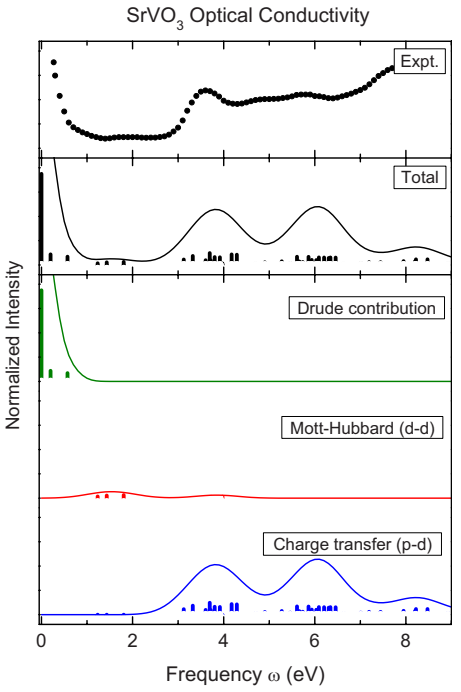

FIG. 6. (Color online) Different contributions to the calculated optical conductivity of $SrVO_3$ compared to the experimental spectrum. The charge-transfer transitions are much stronger and dominate the spectra at higher energies.

of $SrVO_3$-$CaVO_3$-$LaVO_3$-YVO_3. The O 1*s* XAS spectra were shifted by 525.5 eV to take into account the O 1*s* binding energy and the charge-transfer onset. The O 1*s* XAS spectra correspond closely to the charge-transfer transitions in the optical conductivity. This fact was already noticed in the O 1*s* XAS and optical-conductivity spectra of the $Y_{1-x}Ca_xVO_3$ series.[14] This is reasonable because both spectra correspond to transitions to unoccupied states in the conduction band. The difference is that in O 1*s* XAS spectra the electron comes from the O 1*s* core level whereas in the optical conductivity the electron comes mostly from the nonbonding O 2*p* band. Further, we note that this correspondence seems to be a universal characteristic of transition-metal oxides. This can be corroborated comparing the core-level and valence-band spectra of cuprates,[4,9] manganites,[5,10] and vanadates.[6,12]

E. Comparison with DMFT

These materials were initially described using the Hubbard model at half filling within the DMFT approximation. The electronic structure was described in terms of the lower Hubbard band, the quasiparticle peak, and the upper Hubbard band.[11] Within this model, the Drude peak was attributed to intraband quasiparticle excitations, and the higher-energy structures to transitions involving the Hubbard bands.[11] Figure 6 shows the different contributions to the calculated optical conductivity of $SrVO_3$. The present results indicate that, besides the Drude contribution and the Mott-Hubbard *d*-*d* transitions, the charge-transfer transitions are much stronger and dominate the spectra at higher energies. Further, the crystal field and exchange interactions within the V 3*d* bands determines the shape of these transitions.

V. SUMMARY AND CONCLUSION

In summary, we studied the core-level and valence-band optical spectra of $SrVO_3$-$CaVO_3$-$LaVO_3$-YVO_3. The experimental data was analyzed using an extended *p*-*d* cluster model solved by exact diagonalization methods. The O 1*s* x-ray absorption spectra correspond to transition from the O 1*s* core level to unoccupied O 2*p* states whereas the optical-conductivity spectra are related to transitions from the valence to the conduction band. There is a correspondence between the charge-transfer region of the O 1*s* XAS and the optical-conductivity spectra. These charge-transfer transitions are mostly dominated by crystal field and exchange interaction within the V 3*d* band.

[1] E. Dagotto, Rev. Mod. Phys. **66**, 763 (1994).
[2] J. M. D. Coey, M. Viret, and S. von Molnar, Adv. Phys. **48**, 167 (1999).
[3] M. Imada, A. Fujimori, and Y. Tokura, Rev. Mod. Phys. **70**, 1039 (1998).
[4] C. T. Chen, F. Sette, Y. Ma, M. S. Hybertsen, E. B. Stechel, W. M. C. Foulkes, M. Schulter, S.-W. Cheong, A. S. Cooper, L. W. Rupp, Jr., B. Batlogg, Y. L. Soo, Z. H. Ming, A. Krol, and Y. H. Kao, Phys. Rev. Lett. **66**, 104 (1991).
[5] M. Abbate, F. M. F. de Groot, J. C. Fuggle, A. Fujimori, O. Strebel, F. Lopez, M. Domke, G. Kaindl, G. A. Sawatzky, M. Takano, Y. Takeda, H. Eisaki, and S. Uchida, Phys. Rev. B **46**, 4511 (1992).
[6] I. H. Inoue, I. Hase, Y. Aiura, A. Fujimori, K. Morikawa, Y. Haruyama, T. Maruyama, and Y. Nishihara, Physica C **235-240**, 1007 (1994).
[7] I. A. Nekrasov, G. Keller, D. E. Kondakov, A. V. Kozhevnikov, Th. Pruschke, K. Hel4, D. Vollhardt, and V. I. Anisimov, Phys. Rev. B **72**, 155106 (2005).
[8] R. J. O. Mossanek and M. Abbate, Phys. Rev. B **76**, 035101 (2007).
[9] S. Uchida, T. Ido, H. Takagi, T. Arima, Y. Tokura, and S. Tajima, Phys. Rev. B **43**, 7942 (1991).
[10] J. H. Jung, K. H. Kim, D. J. Eom, T. W. Noh, E. J. Choi, Jaejun Yu, Y. S. Kwon, and Y. Chung, Phys. Rev. B **55**, 15489 (1997).
[11] M. J. Rozenberg, G. Kotliar, H. Kajueter, G. A. Thomas, D. H. Rapkine, J. M. Honig, and P. Metcalf, Phys. Rev. Lett. **75**, 105 (1995).
[12] H. Makino, I. H. Inoue, M. J. Rozenberg, I. Hase, Y. Aiura, and S. Onari, Phys. Rev. B **58**, 4384 (1998).
[13] M. Kasuya, Y. Tokura, T. Arima, H. Eisaki, and S. Uchida, Phys. Rev. B **47**, 6197 (1993).
[14] H. F. Pen, M. Abbate, A. Fuijmori, Y. Tokura, H. Eisaki, S. Uchida, and G. A. Sawatzky, Phys. Rev. B **59**, 7422 (1999).
[15] H. Sawada, N. Hamada, K. Terakura, and T. Asada, Phys. Rev. B **53**, 12742 (1996).
[16] Z. Fang, N. Nagaosa, and K. Terakura, Phys. Rev. B **67**, 035101 (2003).
[17] E. Pavarini, S. Biermann, A. Poteryaev, A. I. Lichtenstein, A. Georges, and O. K. Anderson, Phys. Rev. Lett. **92**, 176403 (2004).
[18] M. De Raychaudhury, E. Pavarini, and O. K. Anderson, Phys. Rev. Lett. **99**, 126402 (2007).
[19] R. J. O. Mossanek, M. Abbate, and A. Fujimori, Phys. Rev. B **74**, 155127 (2006).
[20] P. Lombardo, M. Avignon, J. Schmalian, and K.-H. Bennemann, Phys. Rev. B **54**, 5317 (1996).
[21] G. Sordi, A. Amaricci, and M. J. Rozenberg, Phys. Rev. Lett. **99**, 196403 (2007).
[22] M. Taguchi, A. Chainani, K. Horiba, Y. Takata, M. Yabashi, K. Tamasaku, Y. Nishino, D. Miwa, T. Ishikawa, T. Takeuchi, K. Yamamoto, M. Matsunami1, S. Shin, T. Yokoya, E. Ikenaga, K. Kobayashi, T. Mochiku, K. Hirata, J. Hori, K. Ishii, F. Nakamura, and T. Suzuki, Phys. Rev. Lett. **95**, 177002 (2005).
[23] K. Horiba, M. Taguchi, A. Chainani, Y. Takata, E. Ikenaga, D. Miwa, Y. Nishino, K. Tamasaku, M. Awaji, A. Takeuchi, M. Yabashi, H. Namatame, M. Taniguchi, H. Kumigashira, M. Oshima, M. Lippmaa, M. Kawasaki, H. Koinuma, K. Kobayashi, T. Ishikawa, and S. Shin, Phys. Rev. Lett. **93**, 236401 (2004).
[24] M. Taguchi, A. Chainani, N. Kamakura, K. Horiba1, Y. Takata, M. Yabashi, K. Tamasaku, Y. Nishino, D. Miwa, T. Ishikawa, S. Shin, E. Ikenaga, T. Yokoya, K. Kobayashi, T. Mochiku, K. Hirata, and K. Motoya, Phys. Rev. B **71**, 155102 (2005).
[25] A. E. Bocquet, T. Mizokawa, K. Morikawa, A. Fujimori, S. R. Barman, K. Maiti, D. D. Sarma, Y. Tokura, and M. Onoda, Phys. Rev. B **53**, 1161 (1996).
[26] R. J. O. Mossanek, M. Abbate, T. Yoshida, A. Fujimori, Y. Yoshida, N. Shirakawa, H. Eisaki, S. Kohno, and F. C. Vicentin, Phys. Rev. B **78**, 075103 (2008).
[27] T. Arima and Y. Tokura, J. Phys. Soc. Jpn. **64**, 2488 (1995).